J Solid State Electrochem (2012) 16:3027–3036
DOI 10.1007/s10008-012-1743-2

ORIGINAL PAPER

Electrodeposition of selenium from 1-ethyl-3-methyl-imidazolium trifluromethylsulfonate

A. Abdel Aal · F. Voigts · D. Chakarov · F. Endres

Received: 20 December 2011 / Revised: 23 March 2012 / Accepted: 2 April 2012 / Published online: 20 April 2012

Abstract The electrodeposition of thin selenium (Se) films from 1-ethyl-3-methyl-imidazolium trifluromethylsulfonate at room and elevated temperatures on gold and on copper substrates was studied under open-air conditions. The effect of bath temperature on the composition and structure of the deposited films was examined using cyclic voltammetry, chemical analysis and X-ray diffraction analysis. The obtained results showed that on gold substrate and at room temperature, a reddish Se film grows mainly in amorphous, monoclinic, rhombohedral and hexagonal structure, while at temperatures ≥90 °C, a grayish film of hexagonal and rhombohedral structure is deposited. Photoelectron spectroscopy shows that both films consist of pure Se with only slight surface contaminations by remnants from the electrodeposition. Due to the differences in phase structure and the presence of the monoclinic phase, the reddish films showed higher light absorbance. The band gap of the reddish film is close to that of pure amorphous Se reported in literature. Deposition on copper substrate leads to formation of CuSe and $CuSe_2$ at room temperature and at 70 °C, respectively.

A. Abdel Aal (✉) · F. Voigts · F. Endres (✉)
Institute of Particle Technology,
Clausthal University of Technology,
38678 Clausthal-Zellerfeld, Germany
e-mail: ibrahim.alsayed@tu-clausthal.de
e-mail: frank.endres@tu-clausthal.de

A. Abdel Aal · D. Chakarov
Department of Applied Physics,
Chalmers University of Technology,
412 96 Göteborg, Sweden

A. Abdel Aal
Central Metallurgical Research and Development Institute,
CMRDI,
P.O. 87, Helwan, Cairo, Egypt

Keywords Ionic liquids · Selenium · Electrodeposition · Thin films

Introduction

The deposition of thin Se films has attracted considerable interest for several potential applications like, e.g. in electronic and optoelectronic devices [1, 2]. The deposition of thin Se films is usually done using vacuum techniques, which are slow, discontinuous and lacks some versatility in the case of multi-element layers on substrates of complex shape [3–5]. During the last 20 years, there have been several attempts to develop low-cost methods for the electrodeposition of Se films in aqueous solutions on different substrates [6–9]. Cabral et al. successfully deposited thin Se films on gold in an acidic solution of SeO_2. Lai et al. studied the nucleation and growth of Se electrodeposition on a tin oxide electrode [10, 11]. However, the deposition process is quite complicated due to underpotential deposition and compound formation [10].

Recently, ionic liquids were suggested as solvents for Se deposition. They have usually wide electrochemical windows and extremely low vapour pressures allowing to use them at temperatures above 100 °C [12–14]. Comparing to aqueous solutions, ionic liquids also have sufficiently high specific ionic conductivities and many organic and inorganic compounds can easily be dissolved in them [12–14]. In 1-butyl-1-methyl-pyrrolidinium bis(trifluoromethylsulfonyl) amide, crystalline grey Se could be deposited from $SeCl_4$ at 150 °C [15]. Furthermore, amorphous Se was deposited from $SeCl_4$ in 1-ethyl-3-methylimidazolium tetrafluoroborate/chloride at temperatures >100 °C, whereas high aspect ratio single-crystalline trigonal Se nanorods were made from SeO_2 [16]. Recently, we demonstrated that Se films deposited at room temperature from 1-butyl-1-methylpyrrolidinium trifluromethylsulfonate

in an open-air cell are reddish and amorphous, hexagonal and rhombohedral phases of the element could be observed. On the other hand, grayish films of hexagonal and rhombohedral phases were made in the same liquid at $T \geq 70$ °C [17].

Hence, the phase structure and morphology of the deposited Se films depend on different parameters such as the Se precursor, the ionic liquid and the operating conditions, which makes the process of Se deposition rather complicated. The present study aims to better understand the influence of the ionic liquid cation on the properties of the Se films, and we compare the results with these from a previous study with 1-butyl-1-methyl pyrrolidinium triflurometh ylsulfonate [17]. Furthermore, the electrochemical behavior of H_2SeO_3 in 1-ethyl-3-methyl-imidazolium triflurometh ylsulfonate ([EMIm][CF_3SO_3]) at room and elevated temperatures (70–110 °C) on gold substrates is presented. In addition, we discuss the surface properties and the morphological features of the deposited Se films at different temperatures. We also report on the electrodeposition of Se on copper electrodes at different temperatures.

Experimental

H_2SeO_3 powder (Sigma-Aldrich, 99.99 %) was used as Se source. 1-Ethyl-3-methyl-imidazolium triflurometh ylsulfonate (Merck, 99.99 %) was employed as electrolyte. As in [17], H_2SeO_3 cannot be dissolved in the pure ionic liquid used here, even at higher temperature (>100 °C). Thus, water (1–5 vol.%) was added to the liquid and a H_2SeO_3 concentration of 0.16 M could be obtained after addition of 5 vol.% H_2O.

Cyclic voltammetry (CV) and electrodeposition experiments were carried out under open-air conditions, using a three-electrode cell setup. Platinum was used as the counter and quasi-reference electrode, respectively. Although Pt is not the best choice as quasi-reference electrode, it has the advantage to not react with the Se precursor. Thus, although there can be a potential shift of up to 200 mV, a Pt quasi-reference electrode is a good compromise. Gold substrates from Arrandee (200–300-nm-thick gold films deposited on chromium-covered borosilicate glass) and Cu (99.99 %) sheets were used as working electrodes, respectively. Directly before use, the gold substrates were carefully heated in a hydrogen flame to red glow, the copper sheet electrodes were polished by etching in 5 % HNO_3 and sonicated in isopropanol for 10 min. An electrochemical cell made of polytetrafluoroethylene (Teflon) was clamped over a Teflon-covered Viton o-ring onto the substrate, thus yielding a surface area of 0.6 cm^2. Prior to use, all parts in contact with the solution were thoroughly cleaned in a mixture of 50/50 vol.% H_2SO_4/H_2O_2 followed by refluxing in bi-distilled water. All electrochemical measurements were performed using a VersaStat 263A Potentiostat/Galvanostat (Princeton Applied Research) controlled by PowerCV and PowerStep software. All experiments were performed in a hood under environmental conditions. After deposition, the samples were rinsed copiously with isopropanol to ensure removal of the ionic liquid and subsequently dried under vacuum at room temperature for 120 min.

A high-resolution field emission scanning electron microscope (Carl Zeiss DSM 982 Gemini) was used to investigate the surface morphology of the electrolysis product. X-ray diffractograms of the deposited Se were acquired using a Siemens D-5000 diffractometer with CoKα radiation. The reflectivity of the films was measured using a Cary 5000 Spectrophotometer with external reflectance accessories DRA 2500 Integrating Sphere at room temperature.

X-ray photoelectron spectroscopy (XPS) was performed in an ultrahigh vacuum (UHV) device with a base pressure of 1×10^{-10} hPa using a hemispherical analyzer (Omicron EA 125) in combination with a non-monochromatic X-ray source (Omicron DAR 400). Mg Kα line (photon energy of 1,253.6 eV) was used for all measurements. The photon source and the analyzer are mounted at an angle of 45 ° to the surface normal of the sample. Electrons were recorded by the hemispherical analyzer (entrance diaphragm, 1.5 mm) with a calculated resolution of 0.83 eV for detail and 2.07 eV for survey spectra, respectively. All XPS spectra are displayed as a function of electron binding energy with respect to the Fermi level.

For quantitative XPS analysis, a Shirley background subtraction was performed [18]. Photoelectron peak areas are calculated via mathematical fitting with Gauss-type profiles using OriginPro 7 G including the PFM fitting module, which applies the Levenberg–Marquardt algorithms to achieve the best possible fit to the experimental data. Photoelectric on cross-sections were calculated according to Scofield [19], inelastic mean free paths were calculated according to Seah and Dench [20], asymmetry parameters according Reilman [21]. The transmission function of our hemispherical analyzer has been considered for the determination of stoichiometry.

For all XPS experiments, the sample was mounted on a molybdenum holder and introduced into the UHV by means of a sample transfer system. No additional pretreatment was performed unless stated otherwise. If not otherwise stated, the samples were cleaned by sputtering with Ar^+ ions using an Omicron ISE 5 ion source (2 keV, 10 μA for 60 s).

Results and discussion

Electrodeposition on gold

Electrodeposition at room temperature

Figure 1a represents the electrochemical behavior of 0.16 M H_2SeO_3 in [EMIm][CF_3SO_3]/5 vol.% H_2O on gold at room

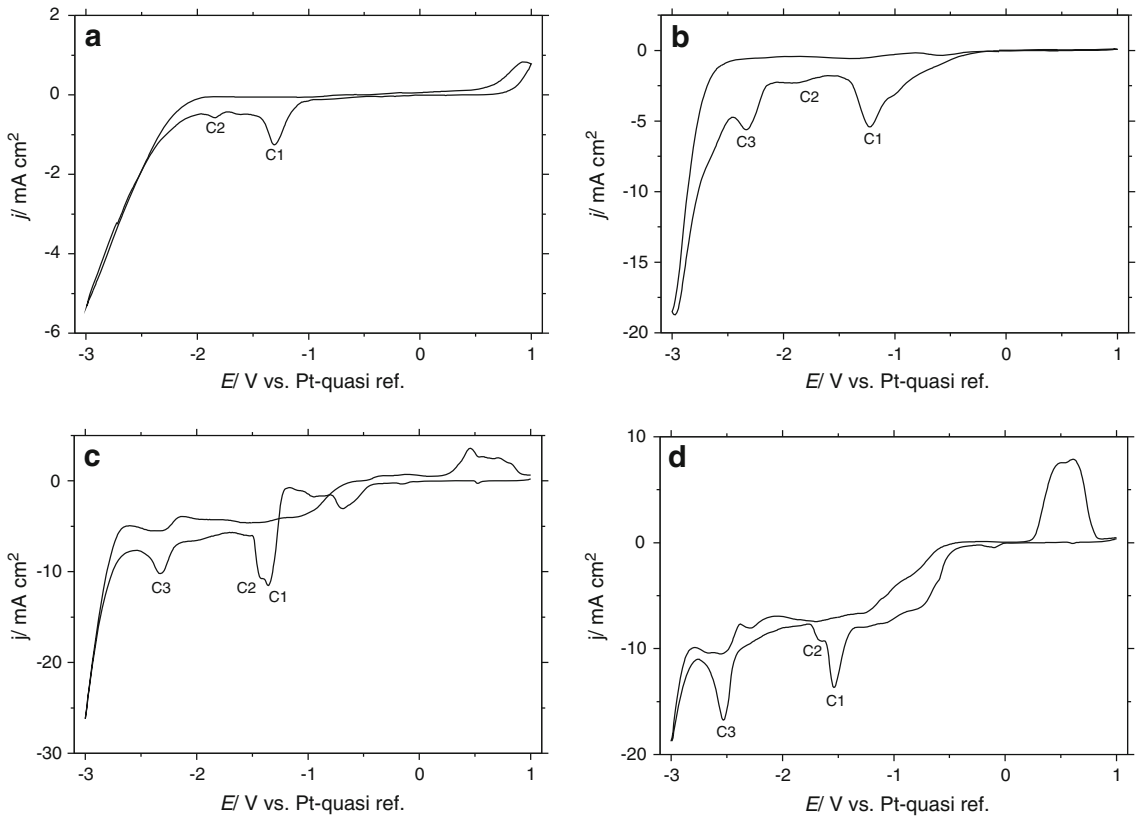

Fig. 1 Cyclic voltammograms of [EMIm][CF_3SO_3]/5 vol.% H_2O with 0.16 M H_2SeO_3 on gold at (**a**) room temperature, (**b**) 70 °C, (**c**) 90 °C and (**d**) 110 °C; scan rate, 10 mV/s vs. Pt-quasi reference electrode

temperature. The cyclic voltammogram shows two cathodic peaks C1 and C2 similar to those ones obtained in an aqueous solution by Lai et al. [11]. They attributed the first cathodic peak to the electroreduction of H_2SeO_3 to Se^0 through a four-electron step (Eq. 1), while the second cathodic peak C2 might be related to the six-electron reduction of H_2SeO_3 to H_2Se (Eq. 2). According to their investigation, H_2Se is subsequently subject to a conproportionation reaction with H_2SeO_3 giving Se^0 (Eq. 3).

$$H_2SeO_3 + 4H^+ + 4e^- \rightleftarrows Se + 3H_2O \qquad E^\circ = 0.50\text{Vvs. SCE} \tag{1}$$

$$H_2SeO_3 + 6H^+ + 6e^- \rightleftarrows H_2Se + 3H_2O \qquad E^\circ = 0.12\text{Vvs.SCE} \tag{2}$$

$$H_2SeO_3 + 2H_2Se \rightleftarrows 2Se + 3H_2O \tag{3}$$

However, the charge involved in peak C1 is much higher than that involved in peak C2, which does not support the above assignments proposed by Lei et al. for aqueous solutions. The Se deposition mechanism in the ionic liquid might therefore be different from that proposed for the aqueous solution. Possible reasons are the influence of solvation layers on the electrochemical reactions and the different chemical nature of ionic liquids [22, 23].

On the other hand, the reduction current observed with the imidazolium ionic liquid is weaker than the previously observed one in the pyrrolidinium liquid [17], but this can be explained on the basis of viscosity differences. Accordingly, the deposition kinetics is different in these ionic liquids which might affect the deposition and growth mechanism of the Se films. This is supported by the observation of Cojocaru and Sima [22]. We have to say clearly that the reduction mechanism of Se in ionic liquids is still not fully understood, thus further investigations are needed.

The X-ray diffraction pattern of the reddish film deposited at C1 is shown in Fig. 2a. The pattern reveals several peaks indicating a crystalline structure of the reddish deposit. These peaks can be assigned to hexagonal (JCPDS 42-1425), monoclinic (JCPDS 24-1202) and rhombohedral (JCPDS 32-0992) Se phases. On the other hand, the reddish color of the deposit attributed to the formation of amorphous red Se cannot be seen in the XRD pattern. It is obvious that the deposit made at room temperature is a mixture of hexagonal, monoclinic and rhombohedral phases, and this

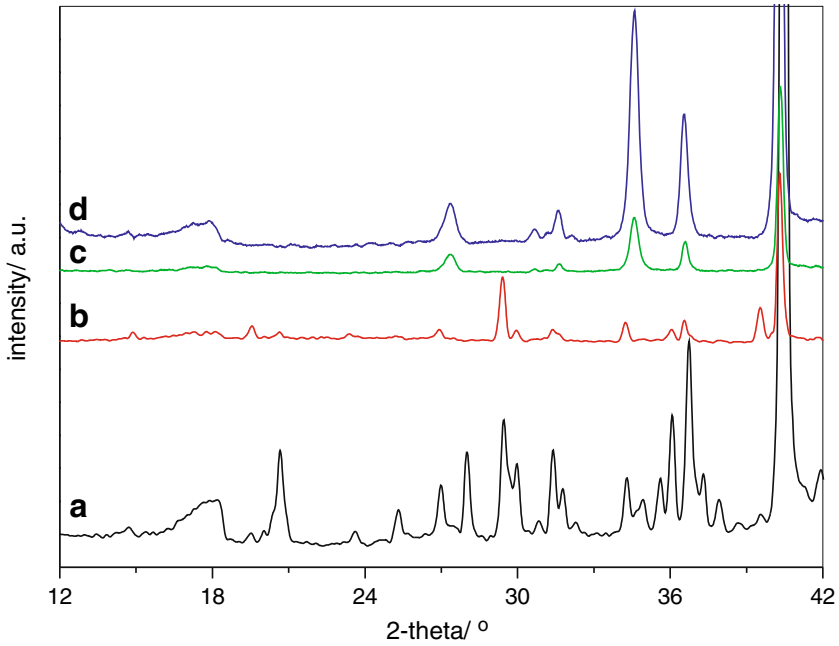

Fig. 2 XRD pattern of a Se film deposited at −1.2 V on gold from [EMIm][CF_3SO_3]/5 vol.% H_2O with 0.16 M H_2SeO_3 at (**a**) room temperature, (**b**) 70 °C, (**c**) 90 °C and (**d**) 110 °C

deposit is polycrystalline in nature. The results clearly indicate that there is no clear distinction between amorphous and vitreous phases of Se. This is in good agreement with Minaev's results who stated that there is no a clear distinction between amorphous and vitreous phases [24]. Our previous results indicated that Se films deposited under similar conditions from an ionic liquid with the pyrrolidinium cation are composed of amorphous, hexagonal and rhombohedral phases [17]. This can be regarded as a hint that the Se phase structure or the growth mechanism depends on the ionic liquid composition.

Figure 3 shows the surface morphology of Se films (with 2-μm thickness) deposited at C1. It was observed that the obtained films are homogeneous, adherent and crack free. The film is likely to grow in different structures as hexagonal platelets (Fig. 3a, b), monoclinic (Fig. 3c) and rhombohedral crystals (Fig. 3d). Obviously, several growth mechanisms occur at the same time.

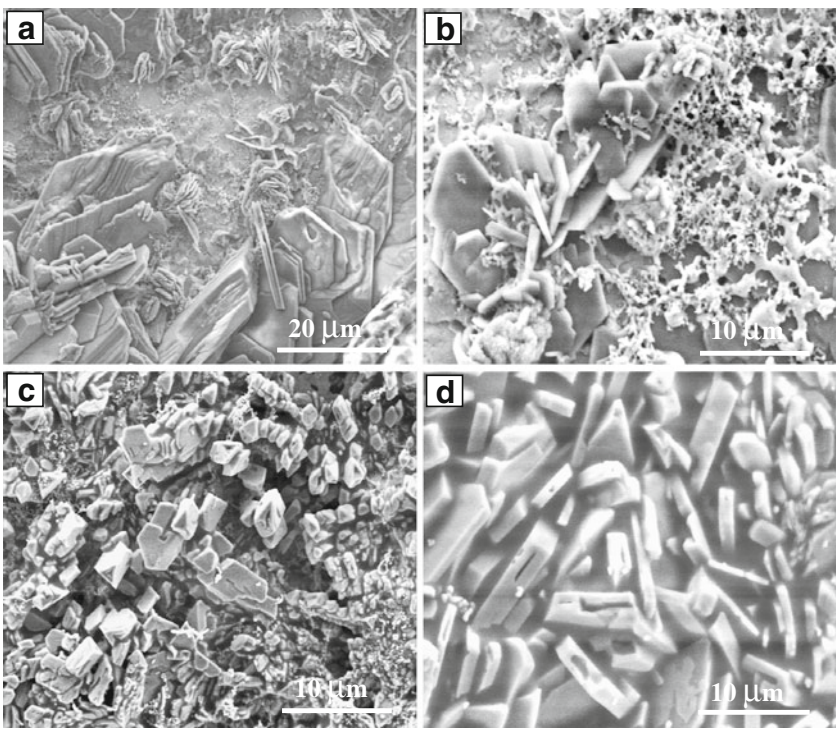

Fig. 3 SEM images of different phases observed in the Se film deposited at −1.2 V on gold from [EMIm][CF_3SO_3]/5 vol.% H_2O with 0.16 M H_2SeO_3 at room temperature

Electrodeposition at elevated temperatures

Figure 1b–d presents the CV recorded on the gold substrate in [EMIm][CF_3SO_3]/5 vol.% H_2O containing 0.16 M H_2SeO_3 at 70, 90 and 110 °C. For the cathodic peak C1 and the small wave at C2, a potential shift compared to the CV recorded at room temperature was observed. At more negative potentials, a third cathodic peak C3 was observed at which the deposited Se is dissolved into the liquid through the reduction of Se^0 to Se^{-2}. In addition, a small shoulder at −0.5 V emerges at 90 °C getting broader at 110 °C. However, no Se deposit was detected at this potential indicating that the reduction product there is a soluble species. An anodic peak in the reverse scan might be related to the dissolution of the deposited Se film, indicating that the Se reduction process is reversible at higher temperatures. It is obvious that the cathodic peaks are shifted with a temperature increase though the voltammogram is still characterized by three cathodic peaks. There is no clear reason for such a behavior, but it might be due to the electrolyte nature and the different stability of the species formed at elevated temperature. The presence of water might also complicate the process. Compared with the previous study of H_2SeO_3 behavior in an ionic liquid with pyrrolidinium cation, the clear differences in the cathodic peak intensity and the potential shifts indicate to a different mechanism of Se deposition in both liquids at elevated temperature [17].

In the following, Se films were deposited at 70, 90 and 110 °C, and the phase structure of the obtained grayish films was analyzed by XRD. The pattern in Fig. 2b illustrates that the deposit at 70 °C is a mixture of monoclinic phase (JCPDS 24-1202) and hexagonal phase (JCPDS 06-0362) with lattice parameters of a=4.37 Å and c=4.95 Å. Besides the diffraction peaks of these two phases, a new strong peak was detected at 2θ = 39.3 ° indicating the formation of a hardly investigated Se (JSPDS-27-0602). Based on the XRD database reported by McCann and Cartz, this phase could not be indexed as cubic or hexagonal, neither did it fit tetragonal and orthorhombic ones [25]. The authors concluded that the diffraction pattern of this phase could not be assigned to a distinct structure. The XRD patterns of the deposited films at temperatures of 90 and 110 °C reveal that a hexagonal phase grows together with a rhombohedral one for both films (Fig. 2c, d). These two phases were also observed for the Se films deposited under similar conditions from an ionic liquid with pyrrolidinium cation [17].

Additionally, the surface morphology of the Se films (with 5-μm thickness) deposited at 70, 90 and 110 °C were investigated as shown in Fig. 4. For all temperatures, the deposited films were found to be adhering, homogeneous and crack free. The SEM micrograph in Fig. 4a shows that the film deposited at 70 °C consists of spherical particles, crystalline flower-like plates with hexagonal sharp edges and colloidal Se which might be related to the questioned Se phase (JSPDS-27-0602). On the other hand, better crystalline films can be observed for the films deposited at 90 and110 °C as shown in Fig. 4b, c.

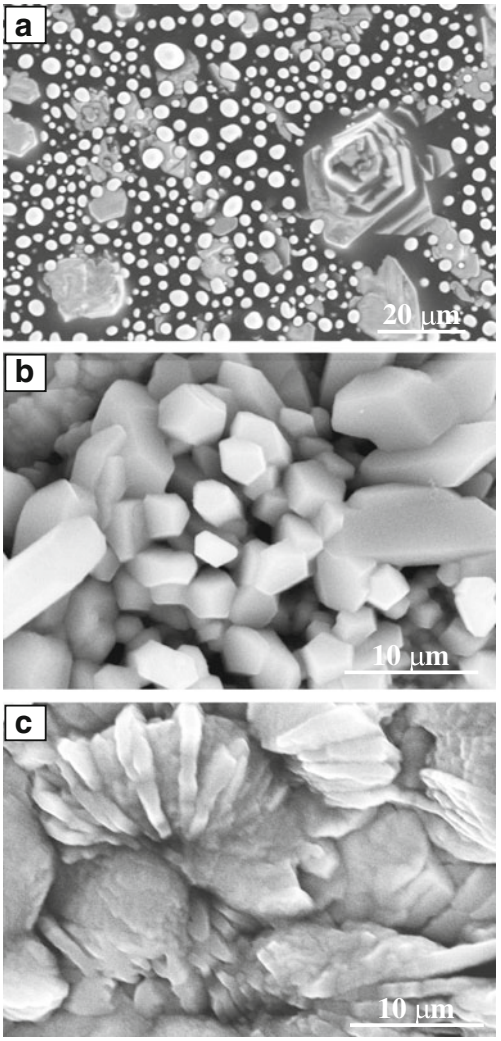

Fig. 4 SEM images of Se films deposited at −1.2 V on gold from [EMIm][CF_3SO_3]/5 vol.% H_2O with 0.16 M H_2SeO_3 at temperatures of (**a**) 70 °C, (**b**) 90 °C and (**c**) 110 °C

Characterization of Se deposits

The optical properties of the reddish and grayish Se films deposited at room temperature and at 110 °C were studied through reflectivity measurements. Figure 7 shows the diffuse reflectance (R) spectra in the visible and near infrared regions. The reddish Se film showed less reflectance (higher absorbance) than the grayish one. This behavior is probably attributed to differences in the phase structure of both films. It is well-known that the monoclinic phase has a higher absorbance than other Se phases, and its presence in the

reddish films might increase the total absorbance of the film [26].

The absorption coefficient and the optical band gap energy were calculated on the basis of the recorded optical spectra as explained in [17, 27–29]. The optical band gap of the deposited reddish film from the inset shown in Fig. 5 is ~2.0 eV, which is in agreement with results reported for a pure amorphous Se (2.0 eV) [30, 31], while the observed band gap of the grayish film is 1.43 eV which is lower than the one reported in literature (1.8 eV) for the pure hexagonal gray Se [32, 33]. This is probably related to the presence of the rhombohedral phase besides the hexagonal one.

XPS results from the reddish Se sample as introduced into the UHV chamber are shown in Fig. 6a. Emissions from the deposited Se layer and from several remnants from the deposition process can be detected. Contributions from oxygen (10 at% of the deposited layer), nitrogen (3 at%) and fluorine (3 at%) can be removed almost completely by a sputter cleaning process as described in the experimental section, during which the carbon fraction in the layer decreases from 48 to 18 at% (Fig. 6c). The small Au 4f emission is due to contributions from the substrate. At 784 eV, a small contribution from impurities can be seen which is not removed by sputtering, though featuring a very small count rate. Another impurity can be detected around 530 eV. These impurities contribute less than 1.5 at% each to the total composition of the layer.

Figure 6b shows results from grayish Se obtained in the same manner as in Fig. 6a. Like on reddish Se, remnants from the deposition process can be detected. The fraction of oxygen (11 at% of the deposited layer) can be removed mainly by sputtering. The carbon contribution is reduced from 46 to 7 at% during sputtering (Fig. 6d). The impurities already mentioned (see Fig. 6a) are detectable here, too, and they contribute less than 1.5 at% each to the composition of the layer and cannot be allocated without doubt.

Figure 7 shows a chemical shift analysis performed on detailed spectra from the Se 3d region for the reddish and the grayish Se films. For this analysis, results from the sputter-cleaned samples are used. The experimental data are shown as black dots while the Gaussians used for the fitting procedure are presented as blue and green lines. The sum of all Gaussians is represented by the bold red line. The function used for Shirley background subtraction is shown as the solid black line at the bottom.

The main double peak is due to emission from the metallic Se $3d_{5/2}$ and Se $3d_{3/2}$ orbitals (blue Gaussians). In addition to these contributions, additional intensity can be detected on the high binding energy side (green Gaussians). This is due to emission from Se 3d orbitals in a different chemical environment (core level shift). The shift amounts to 2.4 eV for the reddish Se and 2.6 eV for the grayish Se, which is too small to originate from a SeO_2 that exhibits a chemical shift of 4.4 eV [34]. It may be due to a surface layer of oxidized $Se^{\delta+}$ with $0 < \delta < 4$. The comparison of the peak areas reveals that 97 % of the red Se in this sample is in the elemental Se^0, while only 3 % is in the oxidized state $Se^{\delta+}$. This is valid for both the reddish and the grayish Se samples, respectively. It can be noted that the Se layers formed in the present work show an almost complete elemental composition, while the layers deposited previously [17] from an ionic liquid with pyrrolidinium cations have a higher amount of oxidized Se, especially for the reddish layer.

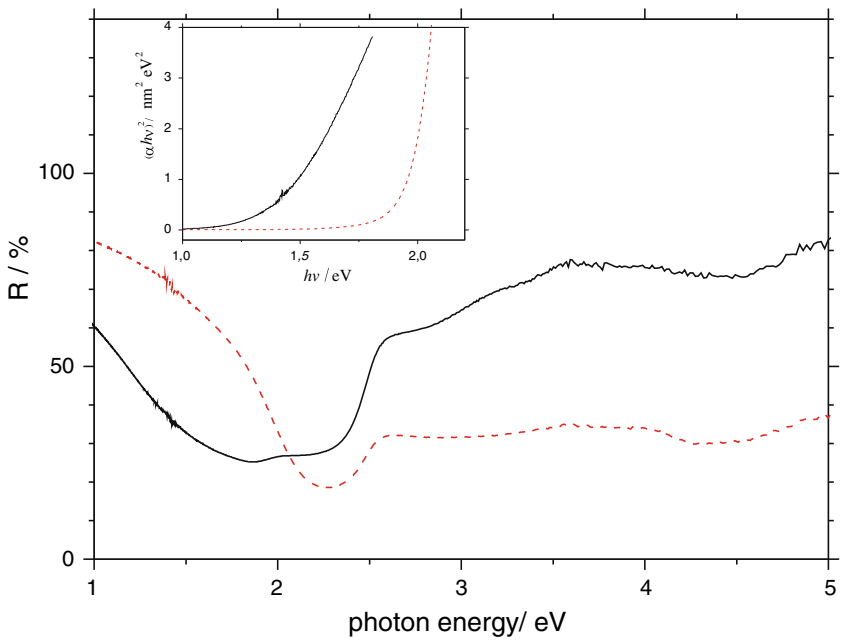

Fig. 5 Reflectivity of reddish (*broken line*) and grayish (*continuous line*) Se films deposited at −1.2 V on gold at room temperature and at a temperature of 110 °C

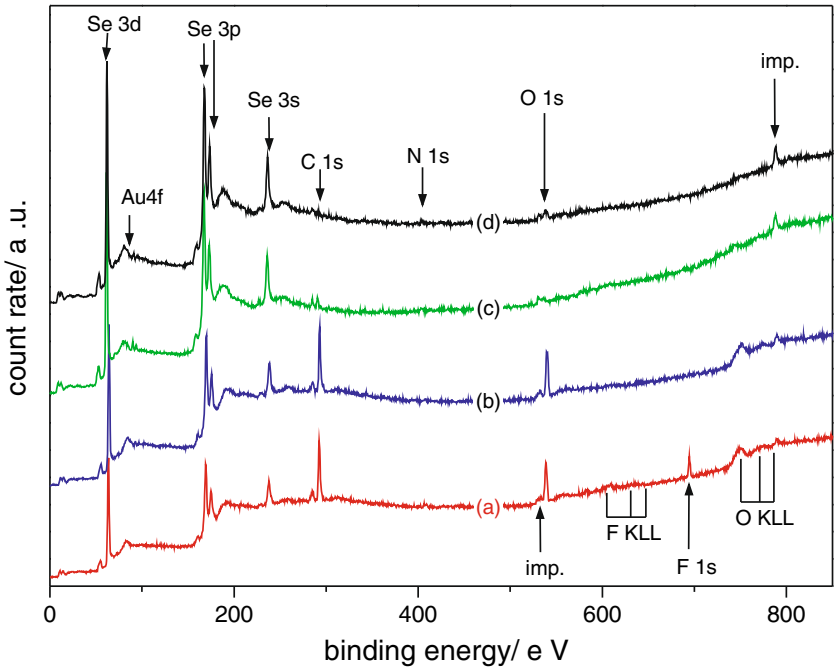

Fig. 6 XPS survey spectra of the (**a**) reddish Se film, (**b**) clean-sputtered grayish Se film, (**c**) clean Ar^+-sputtered reddish Se film and (**d**) Ar^+ clean-sputtered grayish Se film

Electrodeposition of Se on copper

Due to applications of Se films for $CuInSe_2$ solar cells, we investigated the Se deposition on copper substrate, too. Firstly, CV measurements were carried out at room temperature. Figure 8a shows the CV curve of a copper electrode in [EMIm][CF_3SO_3]/5 vol.%H_2O containing 0.16 M H_2SeO_3 at room temperature. One cathodic peak (C1) is detected, at which a black layer is formed. In order to get further information on the layer composition, an XRD analysis of the layer was performed. The pattern in Fig. 9 indicates that the layer is composed of CuSe (JCPDS 20-1020). The pattern also shows a strong Cu peak at 2θ of 50.7 ° corresponding to the substrate. The formation of CuSe is not surprising as the hexagonal α-CuSe is the stable form at room temperature in the phase diagram of the Cu–Se binary system [35]. Furthermore, our results are in a good agreement with literature data confirming the reaction between the copper electrode and Se in aqueous solutions leading to copper–selenides [36–39]. The surface morphology of the deposited layer at

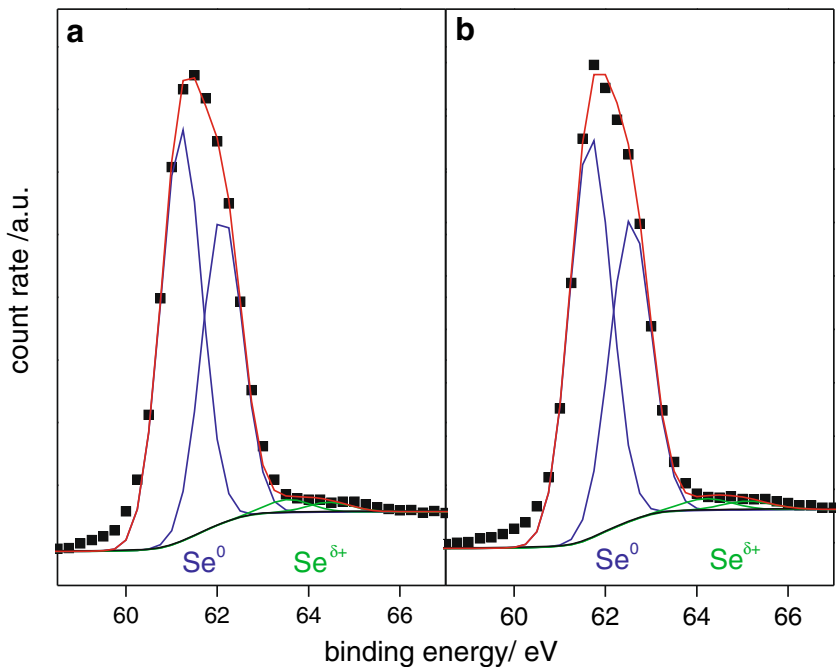

Fig. 7 XPS detail spectra from the Se 3D region of (**a**) the sputter-cleaned reddish Se film and (**b**) the sputter-cleaned grayish Se film. The experimental data are shown as *black dots* while the Gaussians used for the fitting procedure are drawn as *blue* and *green lines*. The sum of all Gaussians is represented by the *bold red line*. The function used for Shirley background substraction is shown as the *solid black line* at the bottom

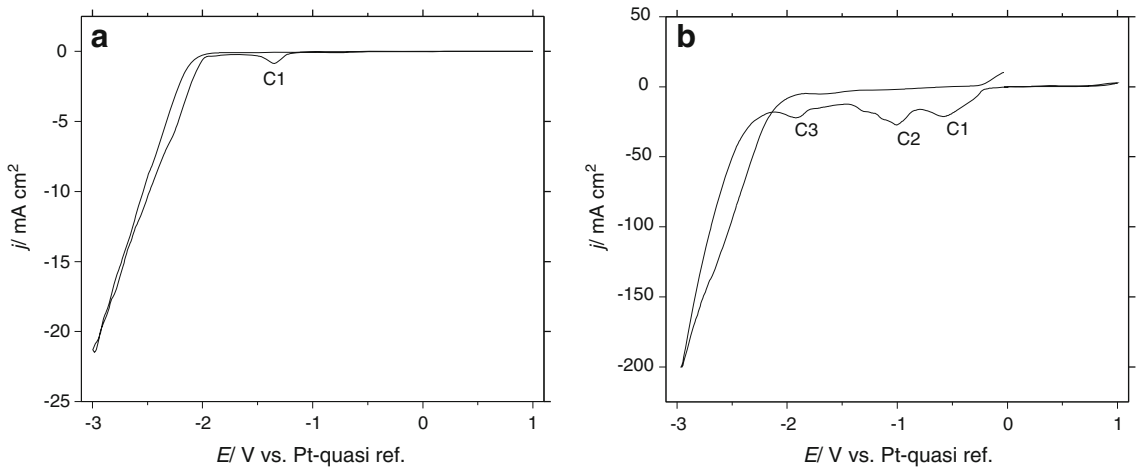

Fig. 8 Cyclic voltammograms of [EMIm][CF_3SO_3]/5 vol.% H_2O **(a)** and [EMIm][CF_3SO_3]/5 vol.% H_2O with 0.16 M H_2SeO_3 on copper at a room temperature **(b)** and at a temperature of 70 °C **(c)**, scan rate 10 mV/s vs. Pt as a quasi-reference electrode

−1.2 V (with 2-μm thickness) was investigated by SEM. The image shows that the black CuSe film has a regular plate-like structure (Fig. 10a). A copper–selenide layer with the same composition was made in an ionic liquid with pyrrolidinium ions [17].

For comparison, a CV measurement was carried out at a temperature of 70 °C, and the recorded voltammogram is presented in Fig. 8b. In contrast to the curve acquired at room temperature, three cathodic peaks are observed. The peaks (C2, C3) are in agreement with the four-electron and six-electron reduction of Se(IV) as shown above for the gold substrate. However, the XRD pattern in Fig. 9 for the film deposited at C2 (−1.2 V) confirmed the formation of $CuSe_2$ (JCPDS 12-0115) and CuSe (JCPDS 20-1020). The crystalline hexagonal Se phase was also identified by comparing the obtained peak at $2\theta = 34.3$ ° with standard data (JCPDS 42-1425). According to the Cu–Se binary phase diagram, $CuSe_2$+Se are formed at a temperature of >65 °C [34]. However, these results are not in agreement with those obtained from pyrrolidinium-based ionic liquid where a copper–selenide layer with $Cu_{1.8}Se$ composition was made [17]. These results lead us to suppose a somewhat different behavior of H_2SeO_3 in the ionic liquid with imidazolium cations compared to a liquid with pyrrolidinium cations.

The deposits of copper–selenide (with 5-μm thickness) were studied by SEM and EDX. As shown in Fig. 10b, the

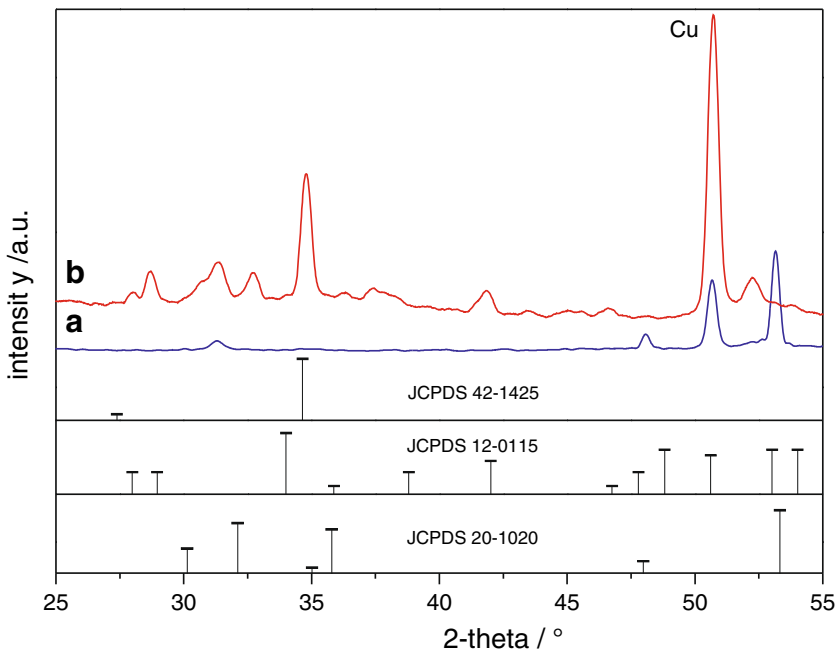

Fig. 9 XRD patterns of a Se film deposited at −1.2 V from [EMIm][CF_3SO_3]/5 vol.%H_2O with 0.16 M H_2SeO_3 at room temperature **(a)** and a temperature of 70 °C **(b)**

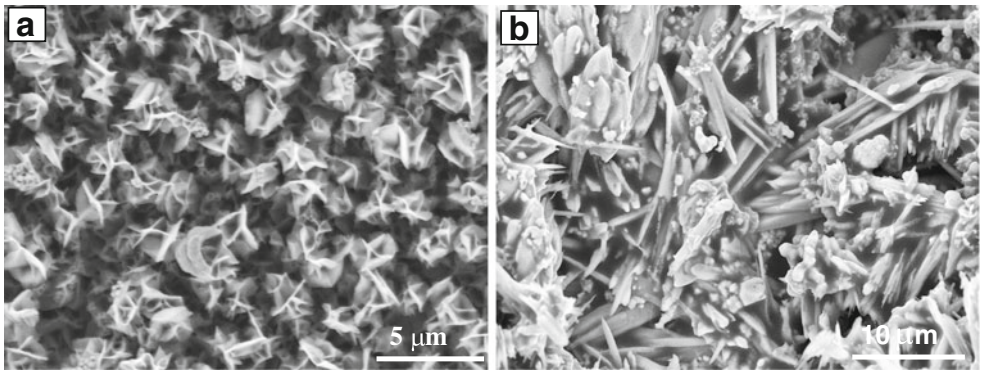

Fig. 10 SEM images of a Se film deposited at −1.2 V from [EMIm][CF_3SO_3]/5 vol.% H_2O with 0.16 M H_2SeO_3 at room temperature **(a)** and a temperature of 70 °C **(b)**

deposited film morphology consists of large needlelike rods with a few micrometers in length. The EDX analysis illustrated that the deposited film consists of Cu and Se. It was also observed that the deposited layer was loosely adhering to copper changing its color to blackish. This copper–selenide probably forms a barrier between the copper and the electrolyte [40, 41]. The origin of the film peeling appears to be related to the deposition of the film simultaneously with the diffusion of copper ions.

Conclusions

In this paper, we have presented the electrodeposition of Se thin films from H_2SeO_3 in 1-ethyl-3-methyl-imidazolium triflurometylsulfonate at room and elevated temperatures on gold and copper substrates. The results indicate the deposition of a reddish Se film with amorphous, monoclinic, rhombohedral and hexagonal phases on gold at room temperature, while hexagonal and rhombohedral phases grow at temperatures of 90–110 °C. The presence of the monoclinic phase with a high absorbance in the reddish deposit might improve the total absorption of the film. The formation of the rhombohedral phase together with the hexagonal one reduces the band gap of the grayish film compared to that one reported in literature for the pure hexagonal gray film. Unlike to aqueous solutions, applying ionic liquids enables Se deposition at higher temperatures (>100 °C) under open-air conditions and leads to the formation of crystalline grayish Se films without any need for post-deposition treatment such as annealing or chemical etching. The reactivity of copper electrodes causes the formation of a CuSe film at room temperature and a $CuSe_2$ film at a temperature of 70 °C during the Se deposition. It should be mentioned that the results are different from our previous study with 1-butyl-1-methylpyrrolidinium trifluoromethylsulfonate showing that the cation might have a certain influence on Se deposition.

Acknowledgement Financial support by the Alexander von Humboldt and German research foundations (DFG) is gratefully acknowledged. The authors gratefully acknowledge experimental assistance by W. Gruber and C. Lehmann from TU Clausthal and by V. Gusak, M. Zäch and C. Langhammer from Chalmers University.

References

1. Chan C, Lam H, Surya C (2010) Sol Energ Mat Sol C 94:207–211
2. Schock H (1996) Appl Surf Sci 92:606–616
3. Pola J, Bastl Z, Slubrt J, Ouchi A (2000) Appl Organometal Chem 14:715–720
4. Bichsel R, Lévy F, Mathieu H (1985) Thin Solid Films 13:87–94
5. Chatterjee E, Gupta S (1986) J Mater Sci Lett 5:559–561
6. Nandhakumar I, Elliott J, Attard G (2001) Chem Mater 13:3840–3842
7. Santos M, Machado S (2004) J Electroanal Chem 567:203–210
8. Solaliendres M, Manzoli A, Salazar-Banda G, Equiluz K, Tanimoto S, Machado S (2008) J Solid State Electrochem 12:679–686
9. Sorenson T, Lister T, Huang M, Stickney J (1999) J Electroanal Chem 146:1019–1027
10. Cabral M, Pedrosa V, Machado S (2010) Electrochim Acta 55:1184–1192
11. Lai Y, Liu F, Li J, Zhang Z, Liu Y (2010) J Electroanal Chem 639:187–192
12. Endres F, MacFarlane D, Abbott A (2008) Electrodeposition from Ionic Liquids. Wiley–VCH, Weinheim
13. Zein El Abedin S, Farag H, Moustafa E, Welz-Biermann U, Endres F (2005) Phys Chem Chem Phys 7:2333–2339
14. Gazlinski M, Lewandowski A, Stepniak I (2006) Electrochim Acta 51:5567–5580
15. Zein El Abedin S, Saad AY, Farag H, Borisenko N, Liu Q, Endres F (2007) Electrochim Acta 52:2746–2754
16. Steichen M, Dale P (2011) Electrochem Commun 13:865–868
17. Abdel Aal A, Voigts F, Chakarov D, Endres F (2012) Electrochim Acta 59:228–236
18. Shirley D (1972) Phys Rev B 5:4709–4714
19. Scofield J (1976) J Electron Spectr Rel Phenom 8:129–137
20. Seah M, Dench W (1979) Surf Interface Anal 1:2–11
21. Reilman R, Msezane A, Manson S (1976) J Electron Spectr Rel Phenom 8:389–394
22. Cojocaru A, Sima M (2012) Rev Chim (Bucharest) 63:217–223
23. Endres F, Höfft O, Borisenko N, Gasparotto L, Prowald A, Al-Salman R, Carstens T, Atkin R, Bund A, Zein El Abedin S (2010) Phys Chem Chem Phys 12:1724–1732
24. Minaev V, Timoshenkova S, Kalugin V (2005) J Optoelectron Adv Mater 7:1717–1741
25. McCann D, Cartz L (1972) J Phys Chem 56:2552–255

26. Prosser V, Henisch K (1966) Mat Res Bull 2:75–83
27. Kubelka P, Munk F (1931) Tech Phys 12:593–601
28. Kubelk P (1948) J Opt Soc Am 38:448–457
29. Pejova P, Grozdanov I (2001) Appl Surf Sci 177:152–157
30. Low H, Sulz G, Lacher M, Kuhner G, Uptmoor G (1992) Sens Actuators B 9:215–219
31. Klober J, Ludwig M, Schneider HA (1991) Sens Actuators B 3:69–74
32. Murty N, Jawalekar S (1983) Thin Solid Films 102:283–289
33. Oyabu T (1982) J Appl Phys 53:2785–2787
34. Shenasa M, Sainkar S, Lichtman D (1986) J Electron Spectr Rel Phenom 40:329–337
35. Dullweber T, Rau U, Miguel A, Noufi R, Hans-Werner S (2000) IEEE Trans Electron Dev 47:2249–2254
36. Mishra K, Rajeshwar K (1989) J Electroanal Chem 271:279–294
37. Skyllas-Kazacos M, Miller B (1980) J Electrochem Soc 127:869–873
38. Pottier D, Maurin G (1989) J Appl Electrochem 19:361–367
39. Ueno Y, Kawai H, Sugiura T, Minoura H (1988) Thin Solid Films 157:159–168
40. Etienne A (1970) J Electrochem Soc 117:870–874
41. Bottecchia O (1998) J Braz Chem Soc 9:515–520